MIXED CONVECTION FLOW OF JEFFREY FLUID ALONG AN INCLINED STRETCHING CYLINDER WITH DOUBLE STRATIFICATION EFFECT

by

Tasawar HAYAT [a,b], Sajid QAYYUM [a], Muhammad FAROOQ [a*], Ahmad ALSAEDI [b], and Muhammad AYUB [a]

[a] Department of Mathematics, Quaid-I-Azam University, Islamabad, Pakistan
[b] Nonlinear Analysis and Applied Mathematics Research Group,
Faculty of Science, King Abdulaziz University, Jeddah, Saudi Arabia

Original scientific paper
https://doi.org/10.2298/TSCI141106052H

This paper addresses double stratified mixed convection boundary layer flow of Jeffrey fluid due to an impermeable inclined stretching cylinder. Heat transfer analysis is carried out with heat generation/absorption. Variable temperature and concentration are assumed at the surface of cylinder and ambient fluid. Non-linear partial differential equations are reduced into the non-linear ordinary differential equations after using the suitable transformations. Convergent series solutions are computed. Effects of various pertinent parameters on the velocity, temperature, and concentration distributions are analyzed graphically. Numerical values of skin friction coefficient, Nusselt, and Sherwood numbers are also computed and discussed.

Key words: *Jeffrey fluid model, stretching cylinder, mixed convection, heat generation/absorption, double stratification*

Introduction

Analysis of non-newtonian fluids is still a topic of great interest. Scientists have stimulated in this field of research due to numerous applications of non-newtonian fluids in pharmaceuticals, physiology, fiber technology, food products, coating of wires, crystal growth, *etc*. Characteristics of non-newtonian fluids can not be described by a single constitutive relationship. Hence various models of non-newtonain fluids have been proposed. Generally the non-newtonian fluids are divided into three main types *i. e*., (1) rate type (2) differential type, and (3) integral type. Rate type fluids describe the behavior of relaxation and retardation times. Maxwell fluid is a subclass of rate type material which exhibits the behavior of relaxation time only. This model does not present the behavior of retardation time. Thus Jeffrey fluid model [1-5] is proposed to fill this void. Jeffrey fluid model characterizes the linear viscoelastic properties of fluids which has wide spread applications in the polymer industries.

The characteristics of flow over a permeable and impermeable stretching surfaces attained lot of interest and inspiration of researchers and scientists due to its numerous applications in the advanced industrial and technological processes. Further such flows with heat and mass transfer are more significant since the quality of final product greatly depends upon the two factors

* Corresponding author, e-mail: hfaroog@yahoo.com

(1) cooling liquid (2) rate of stretching phenomenon. Applications of such phenomenon include chemical processing equipment, food-stuff processing, extrusion process, paper production, cooling of continuous strips or filaments, design of heat exchangers, wire, and fiber coating. Researchers have explored the flow behavior due to stretching phenomenon in various directions. Freidoonimehr *et al*. [6] presented 3-D rotating squeezing nanofluid flow in a channel with stretching wall. Mukhopadhyay [7] examined MHD flow induced by a porous stretching sheet with slip effects and thermal radiation. Hayat *et al*. [8] studied MHD stagnation point flow of second grade fluid past a stretching cylinder. The 3-D MHD flow of viscoelastic fluid past a stretching/shrinking surface with various physical effects was analyzed by Turkyilmazoglu [9]. Mukhopadhyay [10] investigated chemically reactive boundary layer flow past a stretching cylinder saturated with porous medium. Characteristics of heat and mass transfer in MHD flow of viscous fluid over a stretching surface were explored by Sheikholeslami *et al*. [11].

In recent years the deposition of aerosol has a key role in the advanced technological processes. Explicitly the deposition of contaminant particle on the surface of final products has a pivotal role in the electronic industry. Mixed convection (which is a combination of natural and force convections) is one of the main factors which affects the particle deposition. Mixed convection flows appear in many natural, industrial, and engineering processes. Such flows occur in drying of porous solid, nuclear reactors cooled during emergency shutdown, electronic devices cooled by fans, solar power collectors, flows in the atmosphere and ocean, *etc*. Bhattacharyya *et al*. [12] analyzed slip effect in mixed convection flow past a vertical plate. Hayat *et al*. [13] studied melting heat transfer characteristics in the stagnation point flow of Maxwell fluid with mixed convection. The MHD mixed convection flow of viscoelastic fluid past a porous stretching surface was examined by Turkyilmazoglu [14]. Double stratified mixed convection flow of micropolar fluid with chemical reaction was explored by Rashad *et al*. [15]. Rashidi *et al*. [16] studied radiative mixed convection flow of viscoelastic fluid over a porous wedge. Hayat *et al*. [17] presented 3-D radiative mixed convection flow of viscoelastic fluid in the presence of convective boundary condition. Ellahi *et al*. [18] examined mixed convection boundary layer flow over a vertical slender cylinder. Singh and Makinde [19] explored slip effects in mixed convection flow of viscous fluid past a moving plate with free stream.

Stratification is a phenomenon which plays a key role in many natural, engineering, and industrial processes. It arises due to the variations in temperature and concentration or by combining the fluids of different densities. Such phenomenon includes thermal stratification in oceans and reservoirs, heterogeneous mixtures in atmosphere, ground water reservoirs and energy storage. Concentration of the oxygen level becomes low in the lower bottom of the reservoirs due to biological processes. This difficulty can be handled with the implication of thermal stratification. Double stratified flow of nanofluid over a vertical plate was studied by Ibrahim and Makinde [20]. Hayat *et al*. [21] examined radiative flow of Jeffrey fluid past a stretching sheet with double stratification effects. Mukhopadhyay [22] presented thermally stratified MHD flow induced by an exponentially stretching sheet. Influence of double stratification in MHD flow of micropolar fluid was examined by Srinivasacharya and Upendar [23]. Hayat *et al*. [24] studied the stagnation point flow of an Oldroyd-B fluid with thermally stratified medium.

Literature survey indicates that most of the researchers examined the flow behavior of non-newtonian fluids over the stretching sheet. It appears that the behavior of non-newtonian fluids due to a stretching cylinder is not investigated widely. Therefore, the objective of present analysis is to explore the characteristics of double stratified mixed convection flow of Jeffrey fluid past an inclined stretching cylinder. Heat and mass transfer is also considered. Temperature and concentration at the surface and away from cylinder are assumed variable. Convergent

series solutions are developed by homotopy analysis method [25-31]. Behaviors of various pertinent parameters on the velocity, temperature, and concentration distributions are shown graphically. Skin friction coefficient, Nusselt, and Sherwood numbers are computed numerically for different involved parameters.

Mathematical modeling

We consider the steady and incompressible mixed convection flow of Jeffrey fluid past an inclined stretching cylinder fig. 1. Flow analysis is carried out with double stratification and heat generation-absorption. Temperature and concentration at the surface of cylinder are assumed higher than the ambient fluid. Stretching velocity is due to two forces on the cylinder which are equal in magnitude but opposite in direction when origin is kept constant. The conservation laws after using the boundary layer approximations are given:

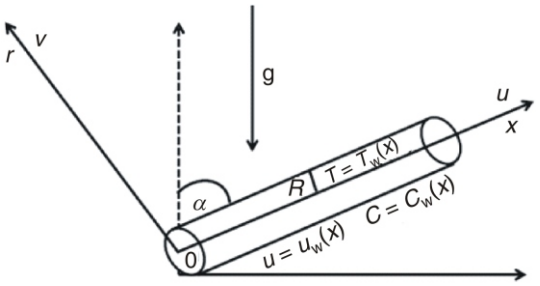

Figure 1. Physical flow problem

$$\frac{\partial (ru)}{\partial x} + \frac{\partial (rv)}{\partial r} = 0 \tag{1}$$

$$u\frac{\partial u}{\partial x} + v\frac{\partial u}{\partial r} = \frac{\nu}{1+\lambda_1}\left(\frac{\partial^2 u}{\partial r^2} + \frac{1}{r}\frac{\partial u}{\partial r}\right) + \frac{\nu\lambda_2}{(1+\lambda_1)}\left(v\frac{\partial^3 u}{\partial r^3} + \frac{\partial v}{\partial r}\frac{\partial^2 u}{\partial r^2} + u\frac{\partial^3 u}{\partial x\partial r^2} + \frac{\partial u}{\partial r}\frac{\partial^2 u}{\partial x\partial r} + \frac{1}{r}v\frac{\partial^2 u}{\partial r^2} + u\frac{\partial^2 u}{\partial x\partial r}\right) + [g\beta_T(T - T_\infty) + g\beta_C(C - C_\infty)]\cos\alpha \tag{2}$$

$$u\frac{\partial T}{\partial x} + v\frac{\partial T}{\partial r} = \frac{k}{\rho c_p}\left(\frac{\partial^2 T}{\partial r^2} + \frac{1}{r}\frac{\partial T}{\partial r}\right) + \frac{Q_0}{\rho c_p}(T - T_\infty) \tag{3}$$

$$u\frac{\partial C}{\partial x} + v\frac{\partial C}{\partial r} = D\left(\frac{\partial^2 C}{\partial r^2} + \frac{1}{r}\frac{\partial C}{\partial r}\right) \tag{4}$$

with the boundary conditions

$$\begin{aligned} &u(x,r) = u_w(x) = \frac{u_0 x}{l}, \quad v(x,r) = 0, T(x,r) = T_w(x) = T_0 + \frac{ax}{l} \\ &C(x,r) = C_w(x) = C_0 + \frac{dx}{l}, \quad \text{at} \quad r = R \\ &u(x,r) \to 0, \quad T(x,r) \to T_\infty = T_0 + \frac{bx}{l}, \quad C(x,r) \to C_\infty = C_0 + \frac{ex}{l} \end{aligned} \tag{5}$$

In the previous expressions u and v are the velocity components in the x and r directions respectively, $\nu = (\mu/\rho)$ is kinematic viscosity, ρ – the fluid density, μ – the dynamic viscos-

ity, λ – the ratio of relaxation to retardation times, λ – the retardation time, g – the acceleration due to gravity, β_T – the thermal expansion coefficient, β_C – the concentration expansion coefficient, α – the angle of inclination, c_p – the specific heat at constant pressure, k – the thermal conductivity, Q_0 – the heat generation/absorption coefficient, $u_w(x)$ – the linear stretching velocity, u_0 – the reference velocity, $T_w(x)$ and $C_w(x)$ are the variable temperature and concentration at the surface of cylinder, and T, T_0, and T_∞ are the fluid, reference, and ambient temperatures, respectively, D – the mass diffusivity, C, C_0, and C_∞ are the fluid, reference, and ambient concentrations, respectively, l – the characteristics length, a, b, d, and e are the dimensional constants. Using the transformations:

$$\eta \quad \sqrt{\frac{u_0}{\nu l}}\ \frac{r^2 \quad R^2}{2R}\ , \quad \theta(\eta) \quad \frac{T \quad T_\infty}{T_w \quad T_0}, \quad \phi(\eta) \quad \frac{C \quad C_\infty}{C_w \quad C_0}$$
$$u \quad \frac{u_0 x}{l} f\ (\eta), \quad v \quad \frac{R}{r}\sqrt{\frac{u_0 \nu}{l}} f(\eta), \quad \psi(\eta) \quad \sqrt{\frac{u_0 \nu x^2}{l}} R f(\eta) \tag{6}$$

Equation (1) is identically satisfied while eqs. (2)-(5) are reduced:

$$\begin{aligned}&(1 \quad 2\gamma\eta) f \quad 2\gamma f \quad (1 \quad \lambda_1)(ff \quad (f\ )^2) \quad \gamma\beta(f f \quad 3 f f\ ) \\ &\beta(1 \quad 2\gamma\eta)((f\ )^2 \quad f f^{iv}) \quad (1 \quad \lambda_1)\lambda_T(\theta \quad N\phi)\cos\alpha \quad 0\end{aligned} \tag{7}$$

$$(1 \quad 2\gamma\eta)\theta \quad 2\gamma\theta \quad \Pr(f\theta \quad f\ \theta \quad Sf \quad \delta\theta) \quad 0 \tag{8}$$

$$(1 \quad 2\gamma\eta)\phi \quad 2\gamma\phi \quad \mathrm{Sc}(f\phi \quad f\phi \quad Pf\ ) \quad 0 \tag{9}$$

$$f(0) \quad 0, f\ (0) \quad 1, \theta(0) \quad 1 \quad S, \phi(0) \quad 1 \quad P, f\ (\eta) \quad 0, \theta(\eta) \quad 0, \phi(\eta) \quad 0, \text{ as } \eta \quad \infty \tag{10}$$

where γ is the curvature parameter, β – the Deborah number in terms of retardation time, λ – the ratio of relaxation to retardation times, λ – the retardation time, Pr – the Prandtl number, Sc – the Schmidt number, δ – the heat generation/absorption parameter, S – the thermal stratification parameter, P – the solutal stratification parameter, λ – the thermal buoyancy (or mixed convection) parameter, and N – the ratio of concentration to thermal buoyancy forces, Gr – the Grashof number due to temperature, Gr^* – the Grashof number due to concentration. These parameters are defined:

$$\begin{aligned}&\gamma \quad \sqrt{\frac{\nu l}{u_0 R^2}}, \quad \beta \quad \frac{\lambda_2 u_0}{l}, \quad \Pr \quad \frac{\mu c_p}{\kappa}, \quad \mathrm{Sc} \quad \frac{\nu}{D}, \quad \delta \quad \frac{l Q_0}{c_p \rho u_0}, \quad S \quad \frac{b}{a}, \quad P \quad \frac{e}{d}, \\ &\lambda_T \quad \frac{\mathrm{Gr}}{\mathrm{Re}^2}, \quad \mathrm{Gr} \quad \nu\frac{g\beta_T(T_w \quad T_0)x^3}{\nu^2}, \quad N \quad \frac{\mathrm{Gr}^*}{\mathrm{Gr}}, \quad \mathrm{Gr}^* \quad \frac{g\beta_C(C_w \quad C_0)x^3}{\nu^2}\end{aligned} \tag{11}$$

Skin friction coefficient, local Nusselt, and Sherwood numbers are defineds:

$$C_f \quad \frac{\tau_w}{\frac{1}{2}\rho u_w^3}, \quad \mathrm{Nu}_x \quad \frac{x q_w}{k(T_w \quad T_0)}, \quad \mathrm{Sh} \quad \frac{x j_w}{D(C_w \quad C_0)} \tag{12}$$

$$\tau_w \quad \frac{\mu}{1 \quad \lambda_1}\frac{\partial u}{\partial r} \quad \lambda_2 \quad v\frac{\partial^2 u}{\partial r^2} \quad u\frac{\partial^2 u}{\partial x \partial r}\Bigg|_{r \quad R}, \quad q_w \quad k\frac{\partial T}{\partial r}\Bigg|_{r \quad R}, \quad j_w \quad D\frac{\partial C}{\partial r}\Bigg|_{r \quad R} \tag{13}$$

In dimensionless form these quantities can be expressed:

$$\frac{1}{2}C_f\sqrt{\mathrm{Re}_x} \quad \frac{1}{1 \quad \lambda_1}[f \quad (0) \quad \beta(\quad f(0)f \quad (0) \quad \gamma f(0)f \quad (0) \quad f \quad (0)f \quad (0)] \qquad \frac{\mathrm{Nu}}{\sqrt{\mathrm{Re}_x}} \quad \theta(0), \quad \frac{\mathrm{Sh}}{\sqrt{\mathrm{Re}_x}} \quad \phi(0) \tag{14}$$

where $\mathrm{Re}_x \quad u_0 x^2/\nu l$ is the local Reynolds number.

Series solutions

Homotopy analysis method was first proposed by Liao in [23] at 1992 which is used for the construction of series solution of highly non-linear problems. It is preferred over the other methods due to the following advantages.

– It does not depend upon the small or large parameters.
– It ensures the convergence of series solutions.
– It provides us great choice to select the base function and linear operator.

To proceed with such method, it is essential to define the initial guess and linear operator. So initial guesses (f_0, θ_0, ϕ_0) and linear operators $(\mathbf{L}_f, \mathbf{L}_\theta \quad \mathbf{L}_\phi)$ for the momentum, energy, and concentration equations are expressed in the forms:

$$f_0(\eta) \quad 1 \quad \exp(\ \eta), \quad \theta_0(\eta) \quad (1 \quad S)\exp(\ \eta), \quad \text{and} \quad \phi_0(\eta) \quad (1 \quad P)\exp(\ \eta) \tag{15}$$

$$\mathbf{L}_f(f) \quad \frac{\mathrm{d}^3 f}{\mathrm{d}\eta^3} \quad \frac{\mathrm{d}f}{\mathrm{d}\eta}, \quad \mathbf{L}_\theta(\theta) \quad \frac{\mathrm{d}^2\theta}{\mathrm{d}\eta^2} \quad \theta \quad \text{and} \quad \mathbf{L}_\phi(\phi) \quad \frac{\mathrm{d}^2\phi}{\mathrm{d}\eta^2} \quad \phi \tag{16}$$

with

$$\mathbf{L}_f[A_1 \quad A_2\exp(\ \eta) \quad A_3\exp(\eta)] \quad 0 \tag{17}$$

$$\mathbf{L}_\theta[A_4\exp(\ \eta) \quad A_5\exp(\eta)] \quad 0 \tag{18}$$

$$\mathbf{L}_\phi[A_6\exp(\ \eta) \quad A_7\exp(\eta)] \quad 0 \tag{19}$$

in which A_i $(i = 1 - 7)$ are the arbitrary constants.

Convergence analysis

The series solutions by homotopy analysis method depend upon the auxiliary parameter, $\hbar$. This auxiliary parameter provides us great freedom to adjust and control the convergence region of the series solutions. Therefore, we have plotted the $\hbar$-curves at the 15th order of approximations in the figs. (2)-(4). It is seen that permissible values of $\hbar_f$, $\hbar_\theta$, and $\hbar_\phi$ are $-0.95 \quad \hbar_f$, $-0.95 \quad \hbar_\theta$ and $-0.95 \quad \hbar_\phi$.

Results and discussion

The main objective of this section is to explore the impacts of various parameters on the velocity, temperature, and concentration distributions. Figure 5 shows the effect of curvature parameter, γ, on the velocity profile. Velocity distribution decreases near the surface of cyl-

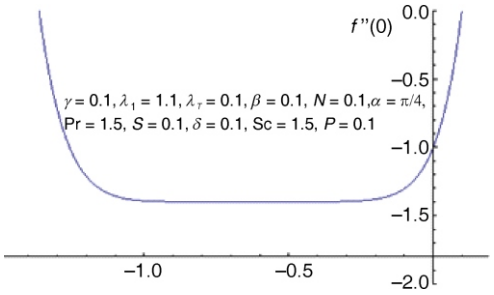

Figure 2. The $\hbar$-curve for f

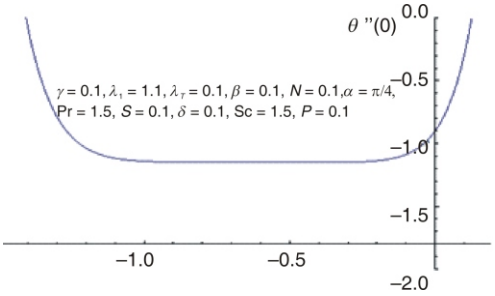

Figure 3. The $\hbar$-curve for θ

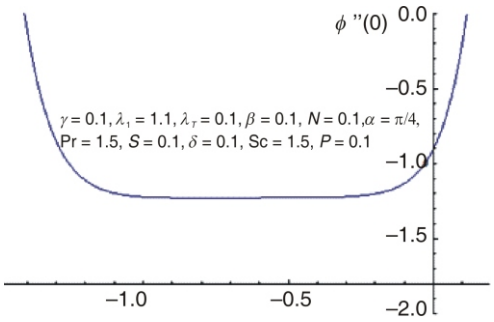

Figure 4. The $\hbar$-curve for ϕ

inder while it increases away from the surface. Velocity curves vanish asymptotically at some large values of η. It is also noted that boundary layer thickness increases. In fact for higher values of curvature parameter the radius of cylinder decreases. So contact surface area of cylinder with the fluid decreases which offers less resistance to the fluid motion. Therefore, velocity profile increases. Influence of λ on velocity distribution is plotted in fig. 6. It is shown that velocity profile decreases for larger values of λ . Since λ is the ratio of relaxation to retardation times so for larger values of λ_1 the relaxation time increases which produces more resistance to the fluid motion. Hence velocity profile decreases. Variation of mixed convection parameter λ_T on velocity profile is sketched in fig. 7. It is analyzed that velocity profile is higher for larger values of mixed convection parameter. It is due to the fact that larger values of mixed convection parameter corresponds to the higher thermal buoyancy force which is responsible in the enhancement of velocity profile. Effect of Deborah number, β, (in terms of retardation time) on velocity distribution is displayed in fig. 8. Velocity and momentum boundary thickness are higher for larger values of β With the increase of β the retardation time increases (or elasticity of the material increases) which is responsible in the enhancement of velocity profile. Figure 9 shows the influence of ratio of buoyancy forces, N,

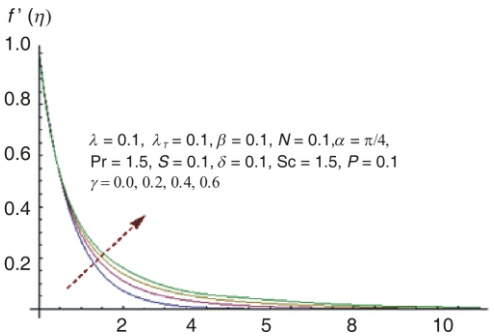

Figure 5. Effect of γ on velocity profile

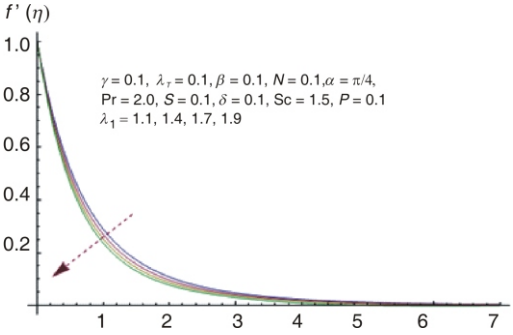

Figure 6. Effect of λ on velocity profile

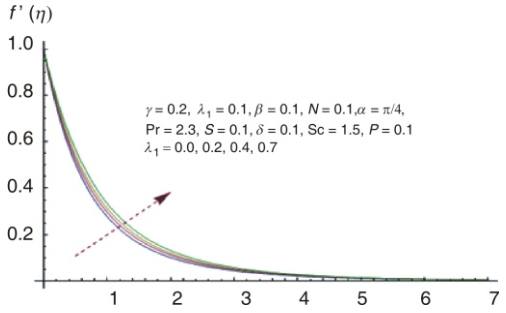

Figure 7. Effect of λ_T on velocity profile

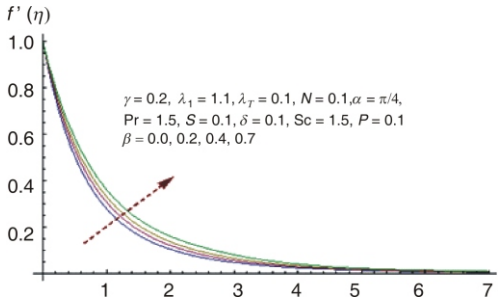

Figure 8. Effect of β on velocity profile

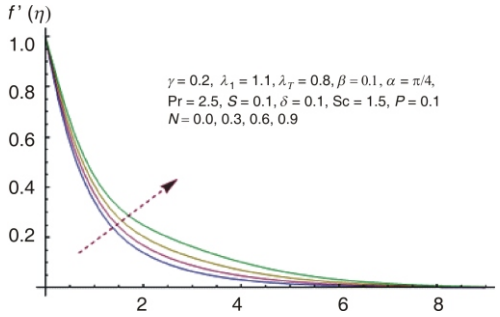

Figure 9. Effect of *N* on velocity profile

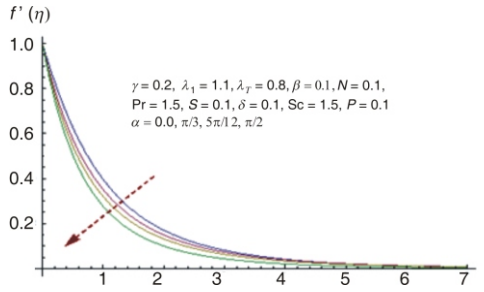

Figure 10. Effect of α on velocity profile

on the velocity distribution. It is noted that velocity profile and momentum boundary layer thickness are higher for larger values of *N*. Since *N* is the ratio of concentration to thermal buoyancy forces so with the increase of *N* the concentration buoyancy force increases which results in the enhancement of velocity profile. Figure 10 displays the effect of angle of inclination, α, on the velocity distribution. It is observed that the velocity profile decreases with an increase in α. Through increase of α the gravity affect decreases which results in the reduction of velocity profile. Variation of thermal stratification parameter *S* on velocity distribution is sketched in fig. 11. It is analyzed that the velocity and momentum boundary layer thickness decrease with an increase in thermal stratification parameter, *S*. In fact convective potential between the surface of cylinder and ambient fluid decreases. Hence velocity profile decreases. Influence of curvature parameter γ on the temperature profile is displayed in fig. 12. Temperature profile decreases near the surface of cylinder and it increases away from the surface. Figure 13 presents the behavior of mixed convection parameter λ_T on temperature distribution. With the increase of mixed convection parameter λ_T the thermal buoyancy force increases which is responsible for high rate of heat transfer. Therefore, temperature profile decreases. Figure 14 shows the characteristics of Deborah number, β, on the temperature profile.

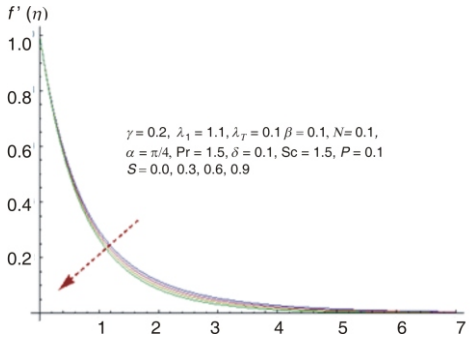

Figure 11. Effect of *S* on velocity profile

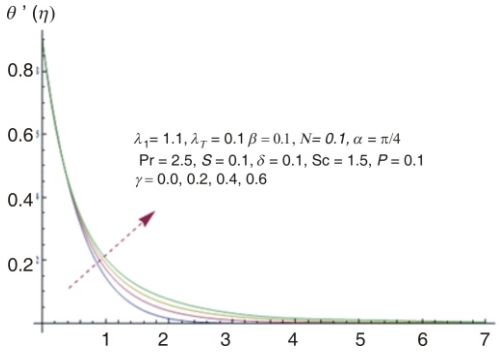

Figure 12. Effect of γ on temperature profile

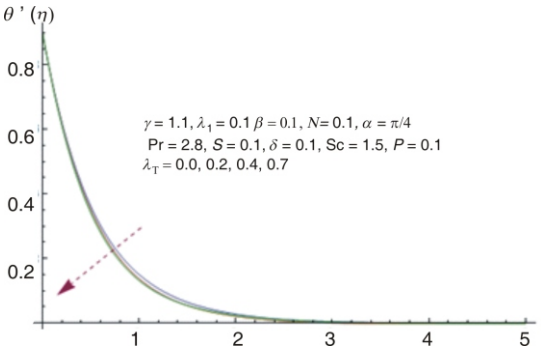

Figure 13. Effect of λ_T on temperature profile

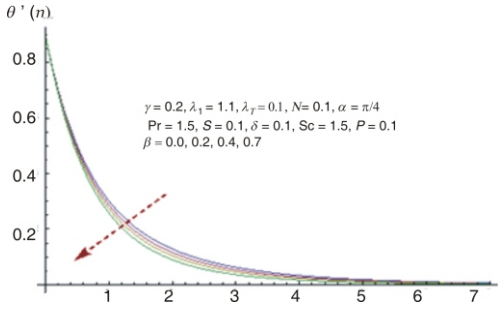

Figure 14. Effect of β on temperature profile

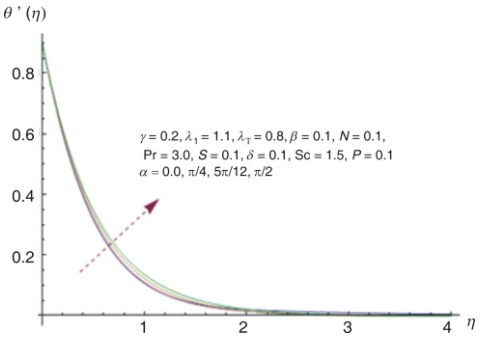

Figure 15. Effect of α on temperature profile

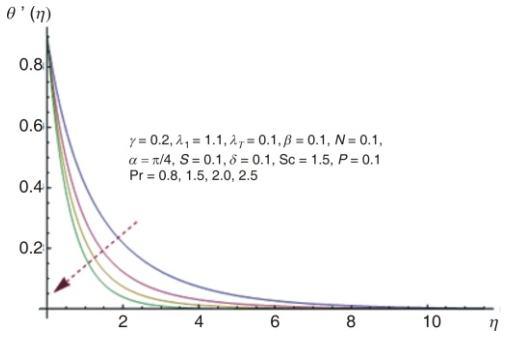

Figure 16. Effect of Prandtl number on temperature profile

Both temperature and thermal boundary layer thickness decrease for higher values of Deborah number, β. Variation of angle of inclination, α, on temperature distribution is expressed in fig. 15. Increase in α shows the increasing behavior of temperature profile. Due to the increase in α the gravity affect decreases which results in the reduction of rate of heat transfer. Therefore, temperature profile increases. Figure 16 provides the analysis for the variation of Prandtl number on the temperature profile. It is noticed that a decrease in the temperature profile and thermal boundary layer thickness is observed when Prandtl number increases. Prandtl number is the ratio of momentum diffusivity to thermal diffusivity. So with the increase of Prandtl number the thermal diffusivity decreases which results in the reduction of temperature profile. Fluids with high Prandtl number corresponds to low thermal diffusivity. Behavior of thermal stratification parameter, S, on the temperature distribution is sketched in fig. 17. Higher values of thermal stratification parameter reduce the temperature and thermal boundary layer thickness. This is due to the fact that the temperature difference gradually decreases between the surface of cylinder and ambient fluid which causes a reduction in the temperature profile. Effect of heat genera-

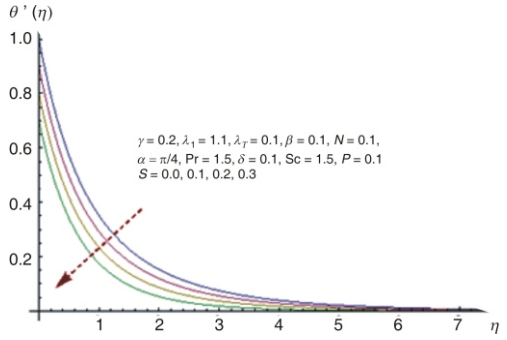

Figure 17. Effect of S on temperature profile

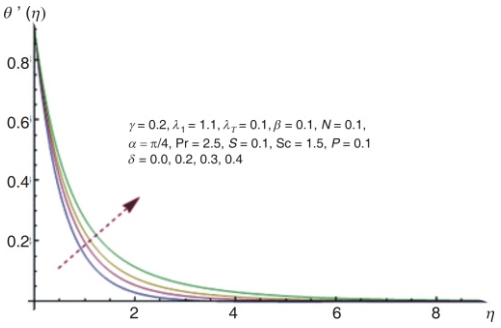

Figure 18. Effect of δ on temperature profile

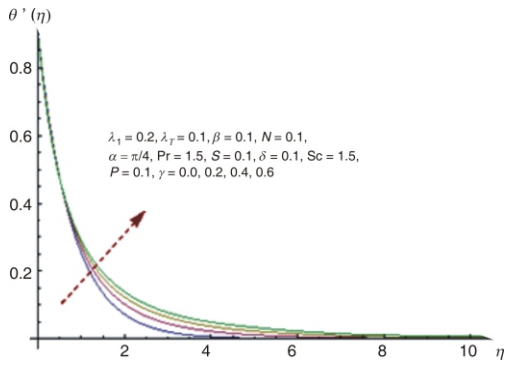

Figure 19. Effect of on concentration profile

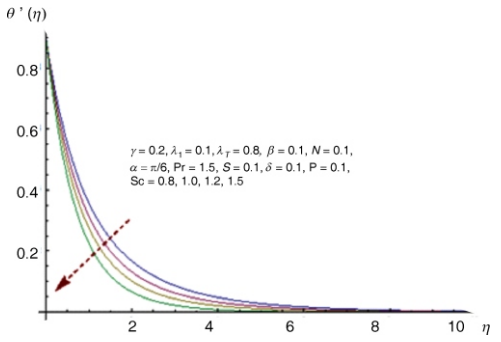

Figure 20. Effect of Schmidt number on concentration profile

tion/absorption parameter, δ, on temperate profile is shown in fig. 18. Both temperature and thermal boundary layer thickness increase when generation/absorption parameter, δ, is increased. Here more heat is produced during the heat generation process which increases the temperature profile. Figure 19 presents the effect of curvature parameter, γ, on concentration distribution. It is observed that concentration profile decreases near the surface of cylinder and it increases away from the surface. Influence of Schmidt number on concentration profiles is sketched in fig. 20. Concentration profile decreases for larger values of Schmidt number. It is the ratio of momentum diffusivity to mass diffusivity. Higher values of Schmidt number corresponds to lower mass diffusivity which results in the reduction of concentration profile. Characteristic of solutal stratification parameter, P, on concentration profile is displayed in fig. 21. Concentration profile decreases when solutal stratification parameter, P, is increased. Further it is also noted that concentration boundary layer thickness decreases. Figures 22 and 23 show the impacts of various parameters on skin friction coefficient. It is analyzed that skin friction coefficient is higher for larger values of α, β, and γ while it decreases with an increase in λ_T.

Table 1 shows the convergence of series solutions for momentum, energy, and concentration equations. It is noted that 26th order of approximation is sufficient for momentum equation and 28th order of approximation is sufficient for energy and concentration equations. Table 2 presents the effects of various parameters on skin friction coefficient. It is noted that skin friction coefficient increases for larger γ, β, α, and S while it decreases with increasing the values of

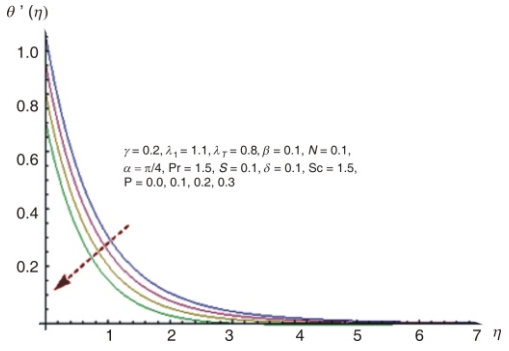

Figure 21. Effect of P on concentration profile

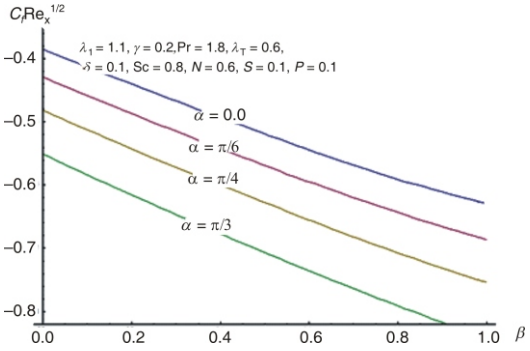

Figure 22. Effect of α and β on skin friction

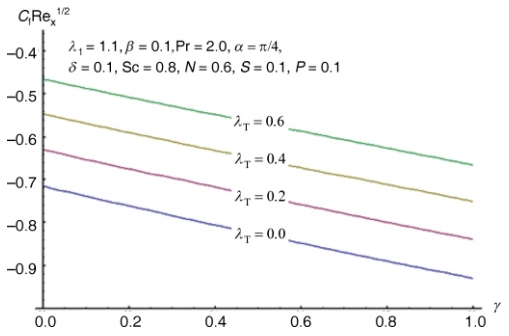

Figure 23. Effect of λ_T and γ on skin friction

Table 1. Convergence of the series solutions for different order of approximations when $\gamma = 0.2$, $\lambda_1 = 1.1, \lambda_T = 0.1, \beta = 0.1, N = 0.1, \alpha =$ /4. Pr = 1.5, $S = 0.1, \delta = 0.1$, Sc = 1.5, and $P = 0.1$

Order of approximation	$f'(0)$	$\theta'(0)$	$\phi'(0)$
1	–1.2666	–1.0613	–1.0950
5	–1.3974	–1.1497	–1.2193
10	–1.3990	–1.1496	–1.2266
15	–1.3984	–1.1484	–1.2279
20	–1.3981	–1.1480	–1.2286
26	–1.3979	–1.1479	–1.2292
28	–1.3979	–1.1478	–1.2294
35	–1.3979	–1.1478	–1.2294

λ_1, λ_T, and N. Negative values of skin friction physically mean that cylinder exerts a drag force on the fluid particles. Table 3 shows the behavior of different parameters on Nusselt number. It is analyzed that Nusselt number increases for higher values of γ, λ_T, β, and Pr while it decreases with an increase in λ, α, S, and δ Table 4 is constructed to examine the behavior of various parameters on Sherwood number. It is observed that Sherwood number increases with the increase in $\gamma, \lambda_T, \beta, N$, and Sc while it decreases when α and P are increased. It is also noted that negative values of Nusselt and Sherwood numbers represent heat and mass transfer from cylinder surface to the fluid *i. e*., normal to the surface.

Concluding remarks

Here we investigated the double stratified mixed convection flow of Jeffrey fluid induced by an impermeable inclined stretching cylinder. Heat transfer characteristics are explored with heat generation/absorption. The key points are summarized as follows:

Velocity, temperature, and concentration profiles increase for larger curvature parameter γ away from the cylinder.

Thermal and solutal stratification parameters reduce the temperature and concentration, respectively.

Higher values of Deborah number result in the enhancement of velocity distribution.

Temperature profile enhances with the increase of heat generation/absorption parameter.

Table 2. Effects of various parameters on the skin friction coefficient when Pr = 1.2, Sc = 1.2, P = 0.1

γ	λ_1	λ_T	β	N	α	S	$-0.5\mathrm{Re}_x^{0.5}C_f$
0.1	1.1	0.1	0.1	0.1	/4	0.1	0.6931
0.2							0.7304
0.5							0.7850
0.2	1.1	0.1	0.1	0.1	/4	0.1	0.7304
	1.2						0.7121
	1.5						0.6643
0.2	1.1	0.1	0.1	0.1	/4	0.1	0.7304
		0.2					0.6999
		0.5					0.6159
0.2	1.1	0.1	0.1	0.1	/4	0.1	0.7304
			0.2				0.7655
			0.5				0.8643
0.2	1.1	0.1	0.1	0.1	/4	0.1	0.7304
				0.2			0.7273
				0.5			0.7198
0.2	1.1	0.1	0.1	0.1	0.0	0.1	0.7174
					/4		0.7304
					/3		0.7394
0.2	1.1	0.1	0.1	0.1	/4	0.1	0.7304
						0.2	0.7345
						0.5	0.7491

Table 3. Effect of various involved parameters on the local Nusselt number when N = 0.1, Sc = 1.2, P = 0.1

γ	λ_1	λ_T	β	α	Pr	S	δ	$-\theta'(0)$
0.0	1.1	0.1	0.1	/4	1.2	0.1	0.1	0.9273
0.2								0.9954
0.3								1.0296
0.2	1.1	0.1	0.1	/4	1.2	0.1	0.1	0.9954
	1.2							0.9873
	1.5							0.9657
0.2	1.1	0.1	0.1	/4	1.2	0.1	0.1	0.9954
		0.2						1.0919
		0.5						1.0649
0.2	1.1	0.1	0.1	/4	1.2	0.1	0.1	0.9954
			0.2					1.0106
			0.5					1.0513
0.2	1.1	0.1	0.1	0.0	1.2	0.1	0.1	1.0064
				/4				0.9954
				/3				0.9857
0.2	1.1	0.1	0.1	/4	0.8	0.1	0.1	0.7687
					1.0			0.8857
					1.2			0.9954
0.2	1.1	0.1	0.1	/4	1.2	0.1	0.1	0.9954
						0.2		0.9640
						0.5		0.8584
0.2	1.1	0.1	0.1	/4	1.2	0.1	0.1	0.9954
							0.2	0.8649
							0.3	0.6771

Skin friction coefficient, Nusselt, and Sherwood numbers increase via curvature parameter.

Higher Prandtl number results in the reduction of temperature profile while Nusselt number increases.

Velocity profile increases while temperature profile decreases when mixed convection parameter – increases.

Nomenclature

a, b, d, e – dimensional constants, [m]
C – fluid concentration, [kgkg^{-1}]
C_f – skin friction, [–]
C_w – wall concentration
C_0 – reference concentraion
C_∞ – ambient concentration, [kgkg^{-1}]
c_p – special heat at constant presure, [Jkg^{-1}°C^{-1}]
D – mass diffusivity, [m^{2}s^{-1}]
f – dimensionless stream function, [–]
Gr – temperature Grashof numbers, [–]
Gr* – concentration Grashof numbers, [–]
g – gravitational acceleration, [ms^{-2}]
$\hbar_\theta$ – auxiliary parameters for temperature, [–]
$\hbar_\phi$ – auxiliary parameters for concentration, [–]
$\hbar_f$ – auxiliary parameter for momentum, [–]

Table 4. Effect of various involved parameters on the Sherwood number when $\lambda_1 = 1.1$, Pr = 1.2, $S = 0.1$, δ

γ	λ_1	β	N	α	Sc	P	$-\phi'(0)$
0.1	0.1	0.1	0.1	$\pi/4$	1.2	0.1	1.0385
0.2							1.0750
0.5							1.1795
0.2	0.1	0.1	0.1	$\pi/4$	1.2	0.1	1.0750
	0.2						1.0948
	0.5						1.1308

γ	λ_1	β	N	α	Sc	P	$-\phi'(0)$
0.2	0.1	0.1	0.1	$\pi/4$	1.2	0.1	1.0750
		0.2					1.0866
		0.5					1.1180
0.2	0.1	0.1	0.1	$\pi/4$	1.2	0.1	1.0750
			0.2				1.0768
			0.5				1.0798
0.2	0.1	0.1	0.1	0.0	1.2	0.1	1.0810
				$\pi/4$			1.0750
				$\pi/3$			1.0707
0.2	0.1	0.1	0.1	$\pi/4$	0.8	0.1	0.8348
					1.0		0.9600
					1.2		1.0750
0.2	0.1	0.1	0.1	$\pi/4$	1.2	0.1	1.0750
						0.2	1.0383
						0.5	0.9233

j_w – mass flux, [kgs^{-1}m^{-2}]
k – thermal conductivity, [Wm^{-1}k^{-1}]
$\mathbf{L}_f$ – linear operator for momentum
$\mathbf{L}_\theta$ – linear operators for energy and concentration
l – characteristics length, [m]
N – concentration to thermal buoyancy ratio
Nu_x – Nusselt number, [–]
Pr – Prandtl number, [–]
Q_0 – heat generation/absorption coefficient, [J]
q_w – surface heat flux, [Wm^{-2}]
P – solutal stratified parameters, [–]
r, x – space co-ordinates, [m]
Re_x – local Reynold number, [–]
S – thermal stratified parameters, [–]
Sc – Schmidt number, [–]
Sh – Sherwood number, [–]
T – fluid temperature, [K]
T_w – wall temperature
T_0 – reference temperature
T_∞ – ambient temperature, [K]
u, v – velocity components, [ms^{-1}]
u_0 – reference velocity, [ms^{-1}]
u_w – stretching surface velocity, [ms^{-1}]
x – stream funtion, [–]

Greeks symbols

α – angle of inclination
β – Deborah number in terms of retardation time, [–]
β_C – solutal expansion coefficient, [–]

β_T – thermal expansion coefficient, [–]
γ – curvature parameter, [–]
δ – heat genearation/absorption| parameter, [–]
η – dimensionless co-ordinate, [–]
q – dimensionless temperature, [–]
ϕ – dimensionless concentration, [–]
λ_T – mixed convection parameter, [–]
l – ratio of relaxation to retardation times, [–]
λ – retardation time, [s]
μ – dynamic viscosit, [$kgm^{-1}s^{-1}$]
ρ – density, [kgm^{-3}]
τ_w – surface shear stress, [Nm^{-2}]
ν – kinematic viscosity, [m^2s^{-1}]
ψ – stream function, [–]
χ – dimensionless variable, [–]

References

[1] Hussain, T., *et al*., Radiative Hydromagnetic Flow of Jeffrey Nanofluid by an Exponentially Stretching Sheet, *Plos one., 9* (2014), 8, pp. e103719
[2] Turkyilmazoglu, M., Pop, I., Exact Analytical Solutions for the Flow and Heat Transfer Near the Stagnation Point on a Stretching / Shrinking Sheet in a Jeffrey Fluid, *Int. J. Heat Mass Transfer., 57* (2013), 1, pp. 82-88
[3] Ellahi, R., *et al*., Blood Flow of Jeffrey Fluid in a Catherized Tapered Artery with the Suspension of Nanoparticles, *Phys. Letter A., 378* (2014), 40, pp. 2973-2980
[4] Hayat, T., *et al*., Three Dimensional Stretched Flow of Jeffrey Fluid with Variable Thermal Conductivity and Thermal Radiation, *Appl. Math. Mech. Engl. Ed., 34* (2013), 7, pp. 823-832
[5] Hayat, T., *et al.*, Thermal Radiation Effects in Squeezing Flow of a Jeffrey Fluid, *Eur. Phys. J. Plus., 128* (2013), 8, p. 85
[6] Freidoonimehr, N., *et al*., Analytical Modelling of Three-Dimensional Squeezing Nanofluid Flow in a Rotating Channel on a Lower Stretching Porous Wall, *Math. Prob. Eng., 2014* (2014), ID692728
[7] Mukhopadhyay, S., Slip Effects on MHD Boundary Layer Flow over an Exponentially Stretching Sheet with Suction/Blowing and Thermal Radiation, *Ain Shams Eng. J., 4* (2013), 3, pp. 485-491
[8] Hayat, T., *et al*., MHD Stagnation Point Flow of Second Grade Fluid over a Stretching Cylinder with Heat and Mass Transfer, *Int. J. Nonlinear Sci. Number. Simul., 15* (2014), 6, pp. 365-376
[9] Turkyilmazoglu, M., Three Dimensional MHD Flow and Heat Transfer over a Stretching/ Shrinking Surface in a Viscoelastic Fluid with Various Physical Effects, *Int. J. Heat Mass Transfer, 78* (2014), Nov., pp. 150-155
[10] Mukhopadhyay, S., Chemically Reactive Solute Transfer in Boundary Layer Flow along a Stretching Cylinder in Porous Medium, *Afr. Mat., 25* (2014), 1, pp. 1-10
[11] Sheikholeslami, M., *et al*., Investigation of Heat and Mass Transfer of Rotating MHD Viscous Flow between a Stretching Sheet and a Porous Surface, *Eng. Comput., 30* (2013), 3, pp. 357-378
[12] Bhattacharyya, K., *et al.*, Similarity Solution of Mixed Convection Boundary Layer Slip Flow over a Vertical Plate, *Ain Shams Eng. J., 4* (2013), 2, pp. 299-305
[13] Hayat, T., *et al*., Melting Heat Transfer in the Stagnation-Point Flow Maxwell Fluid with Double-Diffusive Convection, *International Journal of Numerical Methods for Heat and Fluid Flow, 24* (2014), 3, pp. 760-774
[14] Turkyilmazoglu, M., The Analytical Solution of Mixed Convection Heat Transfer and Fluid Flow of a MHD Viscoelastic Fluid over a Permeable Stretching Surface, *Int. J. Mech. Sci., 77* (2013), Dec., pp. 263-268
[15] Rashad, A. M., *et al*., Mixed Convection Flow of a Micropolar Fluid over a continuously Moving Vertical Surface Immersed in a Thermally and Solutally Stratified Medium with Chemical Reaction, *J. Taiwan Inst. Chem. Eng., 45* (2014), 5, pp. 2163-2169
[16] Rashidi, M. M., *et al*., Mixed Convection Heat Transfer for MHD Viscoelastic Fluid Flow over a Porous Wedge with Thermal Radiation, *Adv. Mech. Eng., 2014* (2014), ID735939
[17] Hayat, T., *et al*., Three-Dimensional Mixed Convection Flow of Viscoelastic Fluid with Thermal Radiation and Convective Conditions, *Plos one., 9* (2014), 3, pp. e90038
[18] Ellahi, R., *et al*., A Study on the Mixed Convection Boundary Layer Flow and Heat Transfer over a Vertical Slender Cylinder, *Thermal Science, 18* (2014), 4. pp. 1247-1258
[19] Singh, G., Makinde, O. D., Mixed Convection Slip Flow with Temperature Jump along a Moving Plate in Presence of Free Stream, *Thermal Science, 19* (2015), 1, pp. 119-128

[20] Ibrahim, W., Makinde, O. D., The Effect of Double Stratification on Boundary Layer Flow and Heat Transfer of Nanofluid over a Vertical Plate, *Computers and Fluids., 86* (2013), Nov., pp. 433-441
[21] Hayat, T., *et al*., Thermal and Concentration Stratifications Effects in Radiative Flow of Jeffrey Fluid over a Stretching Sheet, *Plos one., 9* (2014), Oct., pp. e107858
[22] Mukhopadhyay, S., MHD Boundary Layer Flow and Heat Transfer over an Exponentially Stretching Sheet Embedded in a Thermally Stratified Medium, *Alex. Eng. J., 52* (2103), 3, pp. 259-265
[23] Srinivasacharya, D., Upendar, M., Effect of Double Stratification on MHD Free Convection in a Micropolar Fluid, *J. Egyp. Math. Soc., 21* (2013), 3, pp. 370-378
[24] Hayat, T., *et al*., Thermally Stratified Stagnation Point Flow of an Oldroyd-B Fluid, *Int. J. Nonlinear Sci. Numer. Simulat., 15* (2014), 1, pp. 77-86
[25] Liao, S. J., Homotopy Analysis Method in Non-Linear Differential Equations, Springer and Higher Education Press, Heidelberg, Germany, 2012
[26] Rashidi, M. M., *et al*., Investigation of Entropy Generation in MHD and Slip Flow over a Rotating Porous Disk with Variable Properties, *Int. J. Heat Mass Trans., 70* (2014), Mar., pp. 892-917
[27] Abbasbandy, S., Jalili, M., Determination of Optimal Convergence-Control Parameter Value in Homotopy Analysis Method, *Numer. Algor., 64* (2013), 4, pp. 593-605
[28] Hayat, T., *et al*., Melting Heat Transfer in the Stagnation Point Flow of Powell-Eyring Fluid, *J. Thermophys. Heat Trans., 27* (2013), 4, pp. 761-766
[29] Turkyilmazoglu, M., Solution of the Thomas-Fermi Equation with a Convergent Approach, *Commun. Nonlinear Sci. Numer. Simulat., 17* (2012), 11, pp. 4097-4103
[30] Hayat, T., *et al*., MHD Unsteady Squeezing Flow over a Porous Stretching Plate, *Eur. Phys. J. Plus., 128* (2013), ID157
[31] Hayat, T., *et al*., MHD Flow of Nanofluid over Permeable Stretching Sheet with Convective Boundary Conditions, *Thermal Science, 20* (2016), 6, pp. 1835-1845

Paper submitted: November 6, 2014
Paper revised: March 11, 2015 Paper accepted: March 12, 2015

© 2017 Society of Thermal Engineers of Serbia
Published by the Vinča Institute of Nuclear Sciences, Belgrade, Serbia.
This is an open access article distributed under the CC BY-NC-ND 4.0 terms and conditions